High-glucose toxicity is mediated by AICAR-transformylase/IMP cyclohydrolase and mitigated by AMP-activated protein kinase in *Caenorhabditis elegans*

Received for publication, July 7, 2017, and in revised form, January 29, 2018 Published, Papers in Press, February 2, 2018, DOI 10.1074/jbc.M117.805879

Christin Riedinger[‡1], Michael Mendler[‡1], Andrea Schlotterer[‡], Thomas Fleming[‡], Jürgen Okun[§], Hans-Peter Hammes[¶], Stephan Herzig[‖‡‡], and Peter P. Nawroth[‡**‡‡2]**

*From the [‡]Department of Medicine I and Clinical Chemistry, University of Heidelberg, Im Neuenheimer Feld 410, 69120 Heidelberg, Germany, the [§]Department of Pediatrics, Dietmar Hopp Metabolism Centre, 69120 Heidelberg, Germany, the [¶]V. Medical Hospital, University Hospital Mannheim, Theodor-Kutzer-Ufer 1–3, 68167 Mannheim, Germany, the [‖]Institute for Diabetes and Cancer, Helmholtz Center Munich, Ingolstädter Landstraße 1, 85764 Neuherberg, Germany, the **Joint Heidelberg Institute for Diabetes and Cancer Translational Diabetes Program, Heidelberg University Hospital, Im Neuenheimer Feld 410, 69120 Heidelberg, Germany, and the [‡‡]German Center for Diabetes Research, Ingolstädter Landstraße 1, 85764 Neuherberg, Germany*

Edited by Xiao-Fan Wang

The enzyme AICAR-transformylase/IMP cyclohydrolase (ATIC) catalyzes the last two steps of purine *de novo* synthesis. It metabolizes 5-aminoimidazole-4-carboxamide ribonucleoside (AICAR), which is an AMP analogue, leading to activation of AMP-activated kinase (AMPK). We investigated whether the AICAR–ATIC pathway plays a role in the high glucose (HG)–mediated DNA damage response and AICAR-mediated AMPK activation, explaining the detrimental effects of glucose on neuronal damage and shortening of the lifespan. HG up-regulated the expression and activity of the *Caenorhabditis elegans* homologue of ATIC, C55F2.1 (*atic-1*), and increased the levels of reactive oxygen species and methylglyoxal-derived advanced glycation end products. Overexpression of *atic-1* decreased the lifespan and head motility and increased neuronal damage under both standard and HG conditions. Inhibition of *atic-1* expression, by RNAi, under HG was associated with increased lifespan and head motility and reduced neuronal damage, reactive oxygen species, and methylglyoxal-derived advanced glycation end product accumulation. This effect was independent of an effect on DNA damage or antioxidant defense pathways, such as superoxide dismutase (*sod-3*) or glyoxalase-1 (*glod-4*), but was dependent on AMPK and accumulation of AICAR. Through AMPK, AICAR treatment also reduced the negative effects of HG. The mitochondrial inhibitor rotenone abolished the AICAR/AMPK-induced amelioration of HG effects, pointing to mitochondria as a prime target of the glucotoxic effects in *C. elegans*. We conclude that *atic-1* is involved in glucotoxic effects under HG conditions, either by blocked *atic-1* expression or via AICAR and AMPK induction.

The enzyme AICAR-transformylase/IMP cyclohydrolase (ATIC)[3] catalyzes the last two steps of purine *de novo* synthesis. ATIC metabolizes 5-aminoimidazole-4-carboxamide ribonucleoside (AICAR) to *N*-formyl-5-aminoimidazol-4-carboxamide ribonucleotide (FAICAR) and then to inosine monophosphate (IMP), an analog of AMP. IMP can then be phosphorylated by adenosine kinase to become ZMP, which can bind to the cystathionine-β-synthase domains of the γ-subunit of AMP-activated protein kinase (AMPK), leading to an allosteric change (1). This change makes AMPK a better substrate for its upstream kinases to phosphorylate it at Thr-172 and inhibits dephosphorylation at this site by the protein phosphatases PP2A and PP2C (2, 3). This combined effect significantly increases the activity of AMPK *ex vivo* (4).

Treatment with AICAR has been shown to prevent and/or reverse metabolic syndrome in animal models. In ob/ob mice, fa/fa rats, as well as rats fed a high-fat diet, AICAR treatment has been shown to improve glucose tolerance and whole-body glucose disposal as well as reduce hepatic glucose output and plasma triglycerides and free fatty acids levels (5–8). In streptozotocin-induced diabetic mice, treatment with AICAR increased AMPK activity within the kidney and was linked to reduction in the glomerular matrix and albuminuria (9). Exogenous AICAR can therefore be considered to be an activator of AMPK *in vitro*. However, the regulation of ATIC by endogenous AICAR and its relationship to the activation of AMPK remain unknown, particularly in the context of hyperglycemia and diabetes.

The regulation of AMPK is of great interest in the study of diabetes and metabolic syndrome, as evidence would suggest that loss and/or reduction of AMPK signaling plays an important role in the development of insulin resistance. Upon activa-

This study was supported by the German Research Foundation (DFG, "SFB1118, TP C06 Reactive metabolites as cause of diabetic complications") (to M. M., C. R., T. F., S. H., and P. P. N.) and "SFB1158', TP A03" (to P. P. N.). The authors declare that they have no conflicts of interest with the contents of this article.

This article contains Figs. S1–S7.

[1] Both authors contributed equally to this work.

[2] To whom correspondence should be addressed. Tel.: 49-6221-56-8601; Fax: 49-6221-56-5587; E-mail: peter.nawroth@med.uni-heidelberg.de.

[3] The abbreviations used are: ATIC, AICAR-transformylase/IMP cyclohydrolase; AICAR, 5-aminoimidazole-4-carboxamide ribonucleoside; ZMP, 5-aminoimidazole-4-carboxamide ribonucleotide; IMP, inosine monophosphate; AMPK, adenosine monophosphate kinase; ROS, reactive oxygen species; MG, methylglyoxal; AICARFT, 5-aminoimidazole-4-carboxamide ribonucleotide formyltransferase; HG, high glucose; S, standard; AU, arbitrary unit; AGE, advanced glycation end product; ds-break, double strand break; BHA, butylhydroxyanisol; ctrl, control; tg, transgenic.

tion, AMPK signals through its downstream substrates to restore normal energy levels by stimulating metabolic processes that generate ATP, such as fatty acid oxidation, or by inhibiting those that use ATP, such as triglyceride and protein synthesis (10). The formation of reactive metabolites, such as reactive oxygen species (ROS) and methylglyoxal (MG), are closely linked to energy homeostasis. The normalization of energy levels, induced by AMPK activation, would therefore provide an indirect means of defense against reactive metabolites. Indeed, it has been shown that activation of AMPK can decrease the production of ROS by improving mitochondrial dysfunction *in vitro* and *in vivo* as well in patients with diabetes (11–16). Treatment with AICAR was shown to rescue mitochondrial biogenesis, pyruvate dehydrogenase activity, and mitochondrial complex activity in diabetic kidneys (9). Interestingly, treatment with AICAR also normalized the production of superoxide, which was found to be reduced in the diabetic kidney. This would be consistent with the concept of mitochondrial hormesis, or mitohormesis, in which a degree of ROS production is required within a given biological system to improve systemic defenses against such cellular stressors by inducing an adaptive response (11).

Several studies have shown that DNA damage from reactive metabolites (17–20) plays an important role in the development of late diabetic complications (17, 18, 21–24). Increased damage to the DNA would result in an increased demand on repair processes, in particularly the purine building blocks required for the DNA structure. Within the context of diabetes, this is particularly relevant, as there is evidence to suggest that diabetic patients have inefficient DNA repair (25, 26). Within the context of the ATIC–AICAR pathway, it is conceivable that the activation of ATIC would be protective, as it would provide the necessary pool of purines required for DNA repair. However, in doing so, the endogenous AICAR would be depleted, leading to the loss of AMPK activation and the subsequent beneficial effects of reducing the production and/or consequences of reactive metabolites. The imbalance between the two functions of the ATIC–AICAR pathway may therefore represent an important mechanism for development of the cellular dysfunction observed under hyperglycemic conditions.

In this study, the effect of high glucose on ATIC as well as the effect of AICAR on the activation of AMPK and the production of reactive metabolites and DNA damage was studied. As both AMPK and ATIC are conserved throughout evaluation, *Caenorhabditis elegans* was used as an easily accessible model system.

Results

The *C. elegans* homolog of *atic-1*, C55F2.1, was identified by *in silico* analysis. To verify its enzymatic function, a transgenic nematode (tgC55F2.1b) was created, and the activity of AICAR formyltransferase (AICARFT) was determined. This activity was increased in tgC55F2.1b from 17.2 ± 2.9 μmol/min to 34.2 ± 2.1 μmol/min ($p = 0.003$) compared with the WT, which corresponds well to the activity of the recombinant human protein (to 43.5 ± 1.8 μmol/min, $p = 0.010$) (Fig. 1*A*). A putative methylglyoxal synthase domain was identified within C55F2.1; however, neither the protein extracts of the tg nematodes nor a commercially available purified enzyme of the human homolog enhanced MG production (Fig. 1*B*).

Stimulation of WT nematodes with high glucose (HG), for 5 days, lead to an increase in the expression of *atic-1* of 2.4-fold, as compared with standard (S) conditions ($p < 0.049$) (Fig. 1*C*). This increase in expression was found to persist up to 12 days under HG conditions; however, the effect was not dose-dependent with respect to glucose and not as a consequence of osmotic effects (Fig. S1). The increased expression observed at 5 days of HG was reflected by an increase in AICARFT activity of approximately 2.7-fold compared with S conditions (Fig. 1*D*).

Effect of atic-1 overexpression

The effect of *atic-1* (C55F2.1b) overexpression on lifespan and neuronal damage was determined under standard (S) and HG conditions. Overexpression of *atic-1* decreased the median lifespan from 23.6 ± 0.9 days to 20.6 ± 0.6 days ($p = 0.004$) compared with control nematodes under S conditions (Fig. 2*A*). Under HG, the head motility of the WT nematodes was decreased by 0.03 ± 0.01 mm/s ($p = 0.006$) compared with S conditions (0.016 ± 0.02 m/s). Overexpression of *atic-1* decreased head mobility non-significantly under the S condition by 0.03 ± 0.02 mm/s compared with WT nematodes under S conditions. HG treatment of transgenic nematodes further reduced head motility by 0.08 ± 0.01 mm/s ($p = 0.012$) compared with WT nematodes under HG conditions (Fig. 2*B*). Thus, the effect of HG on head motility was exaggerated in *atic-1*-overexpressing *C. elegans*.

With respect to neuronal damage, HG increased the neuronal damage score from 0.5 ± 0.13 to 1.3 ± 0.23 ($p = 0.010$) in WT nematodes. Overexpression of *atic-1* increased the damage score to 1.2 ± 0.16 ($p = 0.070$) compared with WT nematodes under S conditions. The damage score in *atic-1* transgenic nematodes was not enhanced by HG ($p = 0.761$) (Fig. 2, *C* and *D*). Thus, *atic-1* overexpression under S conditions was able to partially reduce the lifespan, neuronal function, and integrity and increased C55F2.1b mRNA expression (Fig. S2).

Protective effect of atic-1 silencing

The up-regulation of *atic-1* in part mimicked the effects of HG. Therefore, protection from the effect of HG would be expected when the glucose-dependent induction of *atic-1* is inhibited. RNAi treatment of *atic-1* was verified by quantitative PCR and decreased mRNA expression to 24.9% ± 11.3% ($p = 0.003$) under S conditions and to 35.6% ± 14.3% ($p = 0.011$) under HG conditions compared with WT nematodes (Fig. S3). Down-regulation of *atic-1* increased the lifespan under HG conditions from 11.0 ± 0.5 days to 14.7 ± 0.9 days ($p < 0.0001$) (Fig. 3*A*), whereas there was no effect under S conditions ($p = 0.427$, data not shown). The head motility of control RNAi–treated nematodes was decreased under HG conditions, from 0.15 ± 0.01 mm/s to 0.10 ± 0.01 mm/s ($p = 0.019$). Under S conditions, down-regulation of *atic-1* had no effect on head motility compared with control RNAi–treated nematodes. Under HG conditions, down-regulation of *atic-1* prevented the decrease in head motility observed in control RNAi–treated nematodes (Fig. 3*B*). Consistent with the previous finding, HG

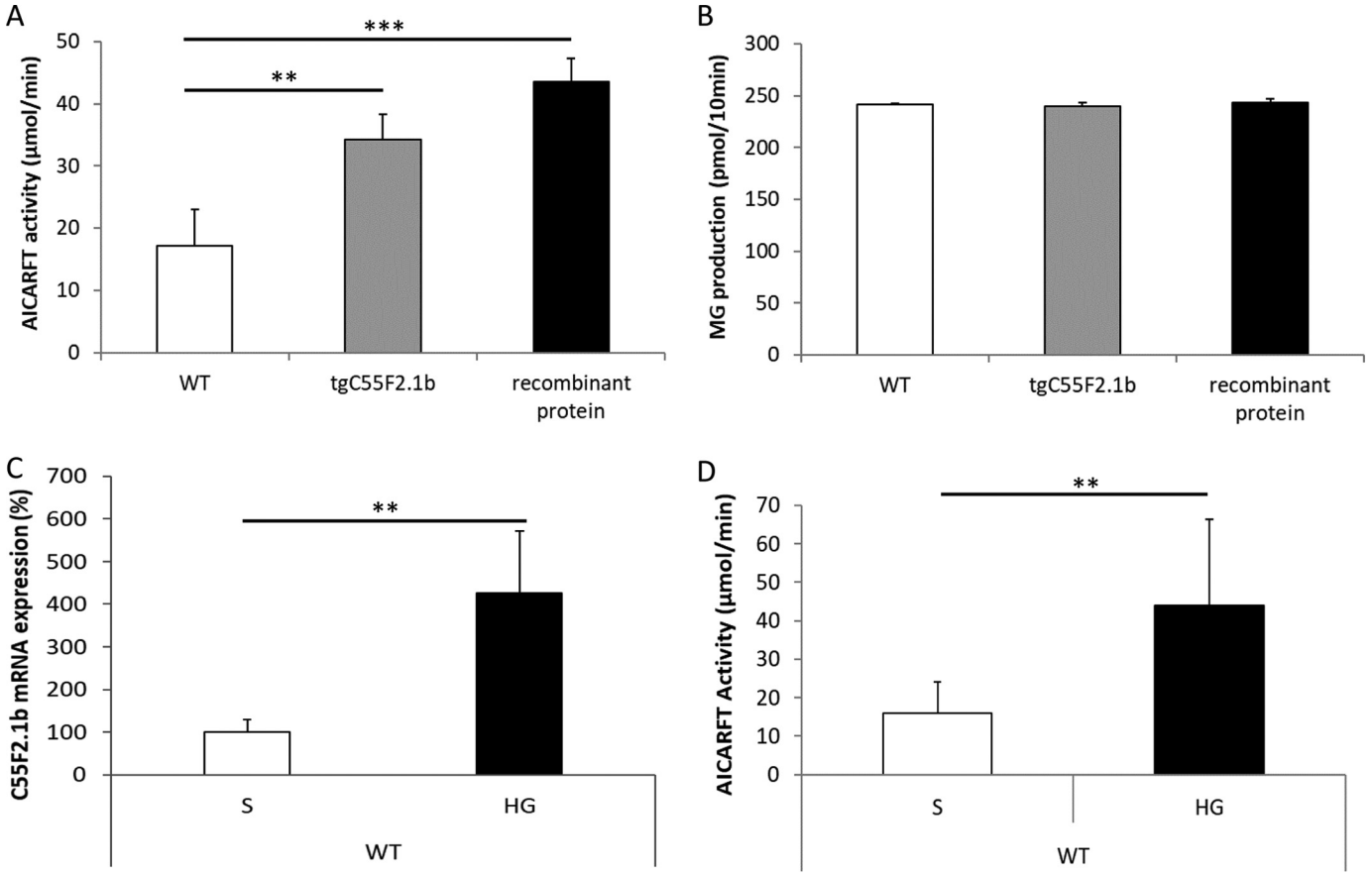

Figure 1. Effect of HG on the *C. elegans* homolog C55F2.1b. *A*, effect of C55F2.1b overexpression on AICARFT activity. AICARFT activity was detected by formation of 10-formyl-tetrahydrofolate in *C. elegans* lysates of WT and transgenic C55F2.1b nematodes as described under "Experimental procedures." Human recombinant protein catalyzed this reaction. Data represent mean ± S.D. of four independent experiments, each with 30 nematodes per group. *B*, effect of C55F2.1b overexpression on MG production. *C. elegans* were cultivated under S conditions. MG production was detected by spectroscopy in lysates of WT, transgenic C55F2.1b nematodes, and recombinant human protein incubated with 2,4-dinitrophenolhydrazine as described under "Experimental procedures." Data represent mean ± S.D. of two experiments, each with 30 nematodes per group. *C*, HG induced C55F2.1b mRNA expression. *C. elegans* were cultured under S and HG conditions, and mRNA expression was quantified by RT-PCR and normalized to *tbg-1* and S as described under "Experimental procedures." Data represent mean ± S.D. of three independent experiments, each performed in triplicate. *D*, effect of HG stimulation on AICARFT activity in nematodes as described under "Experimental procedures." Data represent mean ± S.D. of one experiment with 1000 nematodes per group. **, $p < 0.01$; ***, $p < 0.001$; calculated using unpaired Student's *t* test.

increased the neuronal damage score from 0.82 ± 0.07 to 1.42 ± 0.06 ($p = 0.003$) in control RNAi nematodes, which was prevented by down-regulation of *atic-1* (Fig. 3*C*).

With respect to the formation of ROS and dicarbonyls, HG increased ROS formation in control RNAi nematodes from 59 ± 13 AU/pixel to 222 ± 9 AU/pixel ($p = 0.0001$), which was prevented by down-regulation of *atic-1* (Fig. 3*D*). Similar effects were also observed for the formation of MG-derived AGEs (Fig. 3*E*).

Because AICAR is the substrate of ATIC, it was hypothesized that the beneficial effect resulting from the down-regulation of *atic-1* was mediated by an accumulation of AICAR. There was no significant effect of HG on intracellular AICAR concentration ($p = 0.074$); however, the amount of AICAR was close to the limit of detection. Interestingly, the down-regulation of *atic-1* increased intracellular AICAR by approximately 8-fold under S conditions and approximately 13.1-fold under HG conditions compared with control nematodes. There was no significant difference in intracellular AICAR concentration between the S and HG conditions in *atic-1* RNAi–treated nematodes. This might indirectly reflect the basal turnover of AICAR by *atic-1*, suggesting that the baseline *atic-1*–dependent AICAR turnover is saturated. This would be consistent with the findings observed with overexpression of *atic-1*, which did not show any effect on intracellular AICAR under S or HG conditions compared with control nematodes (Fig. 4*A*).

The inability of HG to reduce AICAR significantly is consistent with the failure of HG to induce DNA double-strand breaks (ds-breaks), as measured by the comet assay. Using bleomycin-treated WT nematodes as a positive control (Fig. 4*B*), it was found that there was no significant difference in ds-break formation between S (Fig. 4*C*) and HG (Fig. 4*D*) conditions (Fig. 4*E*, *third column*). Overexpression of *atic-1* did not reduce the formation of ds-breaks compared with the control under S conditions ($p > 0.05$) (Fig. 4*E*, *fourth column*) but did reduce ds-breaks under HG conditions to 5.6% ($p = 0.002$) (Fig. 4*E*, *fifth column*). Under control RNAi conditions, ds-breaks decreased under S conditions (7.1%, $p = 0.003$) (Fig. 4*E*, *sixth column*), whereas HG did not induce ds-breaks ($p = 0.600$) (Fig. 4*E*, *seventh column*). Down-regulation of *atic-1* increased the formation of ds-breaks under S conditions by 21.9% ($p = 0.003$) (Fig. 4*E*, *eighth lane*), but for unknown reasons, glucose did not

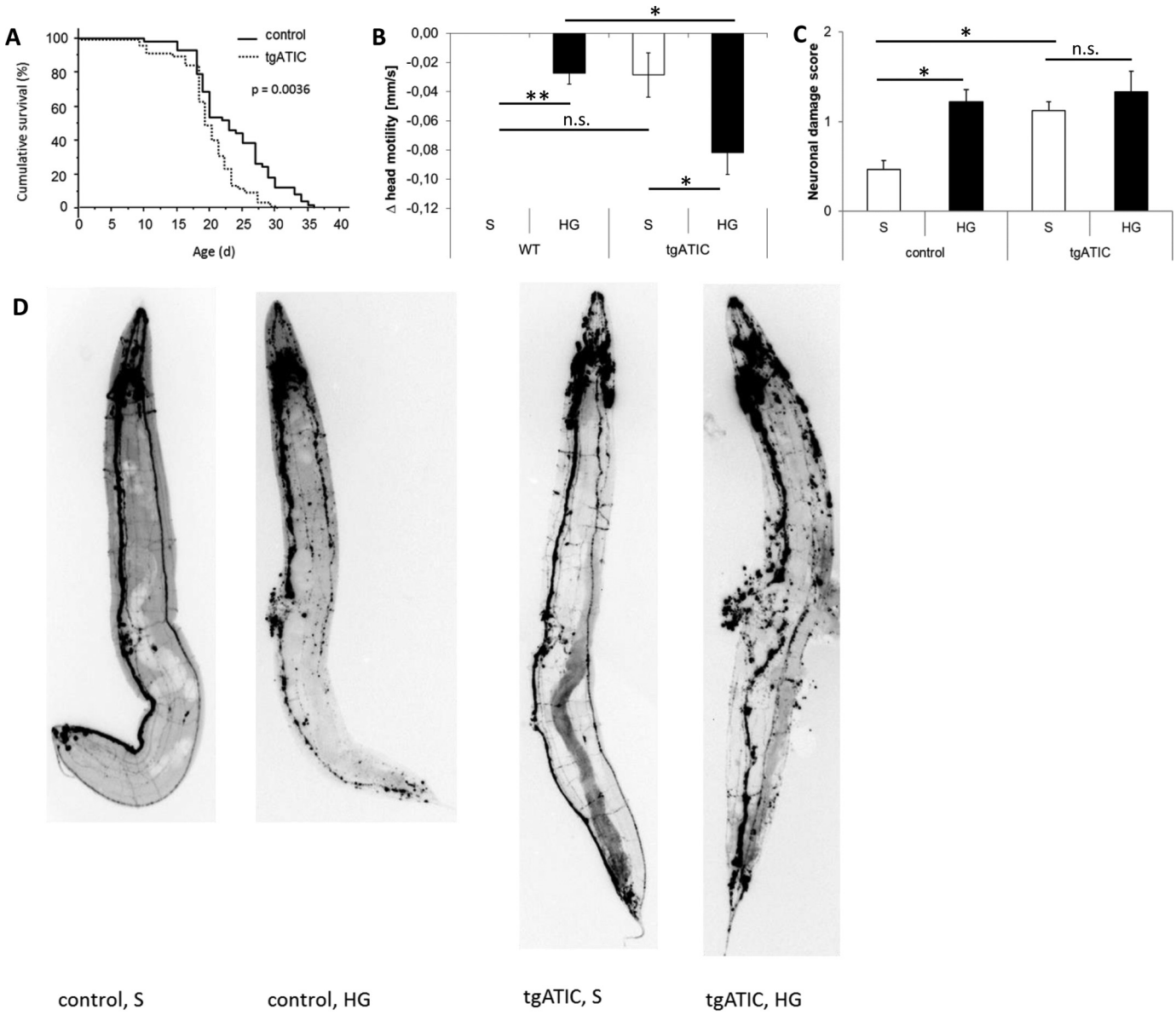

Figure 2. Effect of *atic-1* overexpression on lifespan and neuronal damage. *A*, lifespan of tgATIC (VH2190, *dashed line*) and control (*solid line*) nematodes under S conditions. Shown is one representative of three independent experiments, each with 60 nematodes per group. *B*, head mobility was determined as described under "Experimental procedures." WT and tgATIC (VH2193) *C. elegans* were kept under S and HG conditions as indicated. Data represent mean ± S.D. of three independent experiments, each with 15 nematodes per group. Head motility under S conditions is defined as 0. *, $p < 0.05$; **, $p < 0.01$; *n.s.*, not significant. *C*, neuronal structure was visualized by a pan-neuronal-specific GFP reporter and scored in a blinded procedure as described under "Experimental procedures." Data represent mean ± S.D. of four independent experiments, each with 12 nematodes per group. **, $p < 0.01$, calculated using unpaired Student's *t* test. *D*, neuronal structure was identified by a pan-neuronal-specific GFP reporter. Shown are representative pictures of a single nematode.

increase ds-breaks under HG conditions (14.7%, $p > 0.05$) (Fig. 4*E*, *ninth lane*). This was consistent with HG not exerting its toxic effect in nematodes via genomic DNA damage. Nevertheless, it can be concluded that blocking *atic-1* expression enhanced DNA damage under S conditions, whereas overexpressing *atic-1* reduced DNA damage more under HG. However, as there were no significant differences between S and HG in WT nematodes, HG-mediated *atic-1* induction and DNA damage do not seem to be important pathways when explaining the *atic-1* induction related to the effects of HG.

aak-2–dependent effect of *atic-1* silencing

To establish the potential mechanism for the effect of *atic-1*, the downstream signaling pathway was investigated using *aak-2* nematodes, a homolog of the catalytic subunit of AMPK. It was found that the effects resulting from the down-regulation of *atic-1* under HG conditions were dependent on *aak-2*, as there was no effect resulting from down-regulation of *atic-1* on lifespan in *aak-2* nematodes (Fig. 5*A*). Furthermore, HG-decreased head motility was not improved (Fig. 5*B*). With respect to the formation of reactive metabolites, ROS formation was increased under HG conditions, from 60 ± 10 AU/pixel to 221 ± 3 AU/pixel ($p < 0.0001$), in *aak-2* nematodes and was unaffected by down-regulation of *atic-1* (Fig. 5*C*). Similar results were also found for MG-derived AGEs (Fig. 5*D*). Thus, lack of AMPK abrogated the positive effects of *atic-1* suppression on lifespan, head motility, and reactive metabolite accumulation.

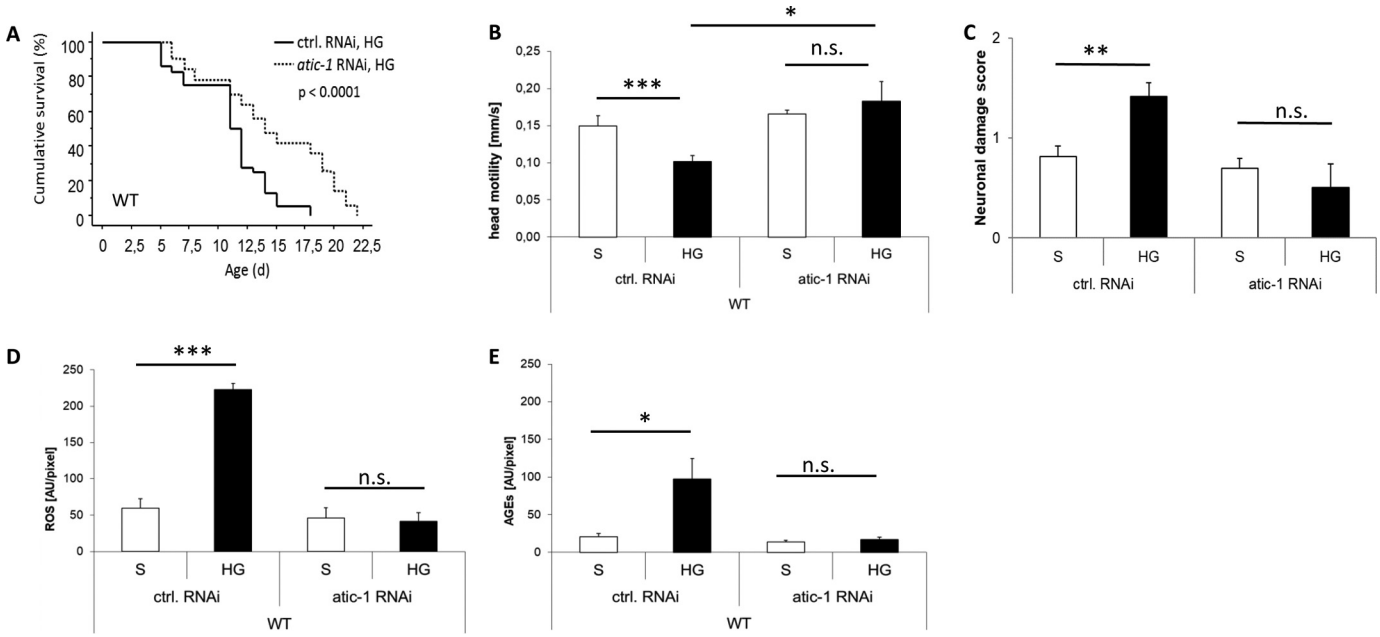

Figure 3. Effect of *atic-1* down-regulation on lifespan, neuronal damage, and reactive metabolites accumulation in *C. elegans*. *A*, effect of *atic-1* down-regulation on lifespan of ctrl (*solid line*) and *atic-1* RNAi (*dashed line*) feeding plates under HG conditions. One representative experiment of three independent experiments is shown, each with 60 nematodes per group. *d*, day. *B*, head motility was determined by video analysis as described under "Experimental procedures" under control RNAi or *atic-1* RNAi, each under S and HG conditions. Data represent mean ± S.D. of three independent experiments, each with 15 nematodes per group. *C*, neuronal structure was visualized by a pan-neuronal-specific GFP reporter and scored in a blinded procedure as described under "Experimental procedures" under S or HG conditions with control or *atic-1* RNAi. Data represent mean ± S.D. of three independent experiments, each with 12 nematodes per group. *D*, ROS formation was detected by confocal laser-scanning microscopy of ethidium-labeled *C. elegans* as described under "Experimental procedures" under S and HG conditions. Data represent mean ± S.D. of three independent experiments, each with 20 nematodes per group. *E*, MG-derived AGE accumulation was detected by immunostaining and quantified as described under "Experimental procedures." Data represent mean ± S.D. of three independent experiments, each with 20 nematodes per group. *, $p < 0.05$; **, $p < 0.01$; ***, $p < 0.001$; calculated using unpaired Student's *t* test. *n.s.*, not significant.

Protective effect of AICAR

As the suppression of *atic-1* increased AICAR levels (Fig. 4*A* and Fig. S4), a pharmacological approach was used to better understand the AICAR effect. Stimulation of WT nematodes with HG for 5 days led to a decrease in AMPK activity, an effect that was partially normalized by the exogenous addition of 1 mM AICAR (Fig. 6*A*).

The HG-mediated decrease in lifespan was also partially normalized by treatment with AICAR, improving the lifespan from 14.0 ± 0.6 days to 20.9 ± 0.8 days ($p = 0.0014$) (Fig. 6*B*, *first group*). This effect was lost when *aak-2* was knocked out ($p = 0.6728$) (Fig. 6*B*, *second group*), whereas loss of the MG- and ROS-detoxifying enzymes *glod-4* ($p = 0.002$) (Fig. 6*B*, *third group*) and *sod-3* ($p = 0.0025$) (Fig. 6*B*, *fourth group*) did not affect prolongation of the lifespan by AICAR. This would suggest that AICAR acts independent of direct detoxification of ROS and dicarbonyls.

Suppression of AMPK by RNAi prevented the AICAR improvement in lifespan under HG conditions (Fig. 6*C*, *first group*). Similar effects were also observed in *glod-4* (Fig. 6*C*, *second group*) and *sod-3* knockouts (Fig. 6*C*, *third group*). Furthermore, double knockout of *glod-4* and *sod-3* did not affect the lifespan prolongation by AICAR under HG conditions (Fig. 6*D*). Similar results were also found for head motility (Fig. 6*E*). HG decreased head motility in the WT to 0.14 ± 0.01 mm/s ($p = 0.0239$), which could be almost normalized by additional AICAR treatment to 0.18 ± 0.01 mm/s ($p = 0.0398$), whereas there was no effect under S conditions ($p = 0.3364$) (Fig. 6*E*, *first group*). This effect of AICAR was lost when *aak-2* was knocked out ($p = 0.7611$) (Fig. 6*E*, *second group*), but loss of *glod-4* ($p = 0.0442$) (Fig. 6*E*, *third group*) and *sod-3* ($p = 0.0138$) (Fig. 6*E*, *fourth group*) did not affect the AICAR effect on head motility under HG conditions.

Neuronal damage was also not affected in a similar manner. The HG-mediated increase in the neuronal damage score to 1.29 ± 0.12 ($p < 0.001$) was normalized by additional AICAR treatment to 0.59 ± 0.13 ($p = 0.0007$), whereas there was no effect under S conditions (Fig. 6*F*, *first group*). This effect was again lost when *aak-2* was down-regulated ($p = 0.0758$) (Fig. 6*F*, *second group*), whereas loss of the MG- and ROS-detoxifying enzymes *glod-4* ($p = 0.0002$) (Fig. 6*F*, *third group*) and *sod-3* ($p = 0.0002$) (Fig. 6*F*, *fourth group*) did not affect the AICAR action of structural damage under HG. Thus, the positive effects of AICAR on head motility, neuronal damage, or lifespan were affected when either *glod-4* or *sod-3* was missing.

Similar data were also obtained with respect to the accumulation of reactive metabolites. ROS formation in WT nematodes was increased to 205.9 ± 8.6 AU/pixel ($p < 0.001$) under HG conditions, and treatment with AICAR partially normalized it to 49.4 AU/pixel ($p < 0.0001$), whereas there was no effect under S conditions ($p = 0.9933$) (Fig. 6*G*, *first group*). The effect of AICAR was lost when *aak-2* was knocked out ($p = 0.8616$) (Fig. 6*G*, *second group*), but loss of the MG- and ROS-detoxifying enzymes *glod-4* ($p < 0.0001$) (Fig. 6*G*, *third group*) and *sod-3* ($p < 0.0001$) (Fig. 6*G*, *fourth group*) did

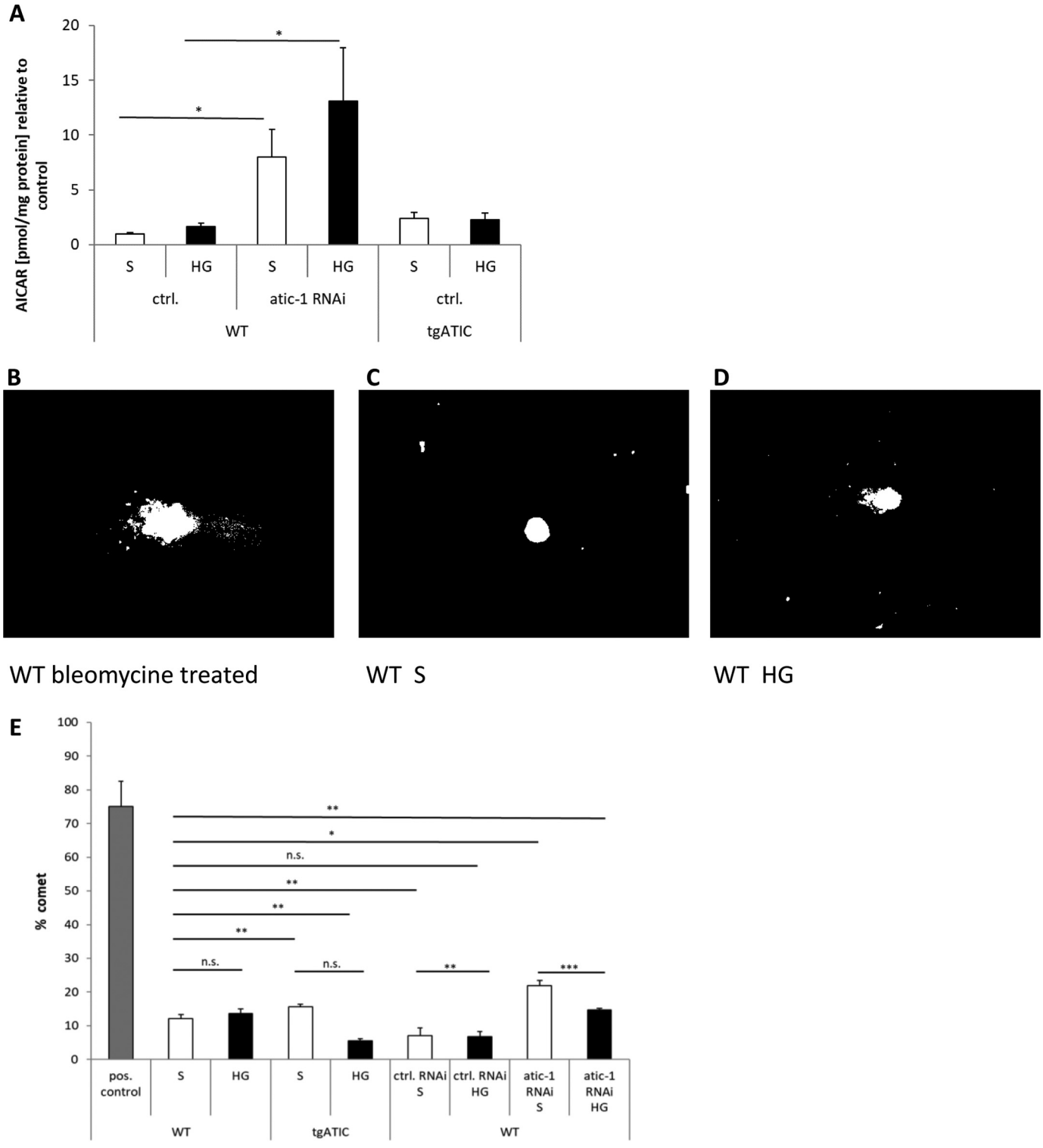

Figure 4. Effect of *atic-1* regulation on AICAR levels determined in a whole-body extract and on DNA damage. *A*, AICAR concentration in whole *C. elegans* extracts was determined as described under "Experimental procedures." WT *C. elegans* were grown on ctrl or *atic-1* RNAi feeding plates, and tgATIC nematodes were grown on control plates. Data represent mean ± S.D. of three independent experiments. *B–D*, comet assay from WT *C. elegans* treated with bleomycin (positive control, *B*) and cultivated under S (*C*) and HG (*D*) conditions. *E*, WT and tgATIC mutant *C. elegans* were cultivated under S and HG conditions. WT *C. elegans* were cultivated on ctrl or *atic-1* RNAi feeding plates. Data represent mean ± S.D. of six independent experiments, each with 70 nematodes per group. *, $p < 0.05$; **, $p < 0.01$; ***, $p < 0.001$; calculated using unpaired Student's *t* test. *n.s.*, not significant.

not affect the AICAR action of ROS formation. Similar results were also obtained for MG-derived AGEs (Fig. 6*H*).

Treatment with AICAR not only affected *sod-3* and *glod-4* independent of the accumulation of reactive metabolites but also the expression of *atic-1* mRNA (Fig. S5). This effect was more pronounced under HG than under S conditions but was most importantly lost in the absence of *aak-2*. Furthermore, knockout of *aak-2* and *sod-3* had no effect on the

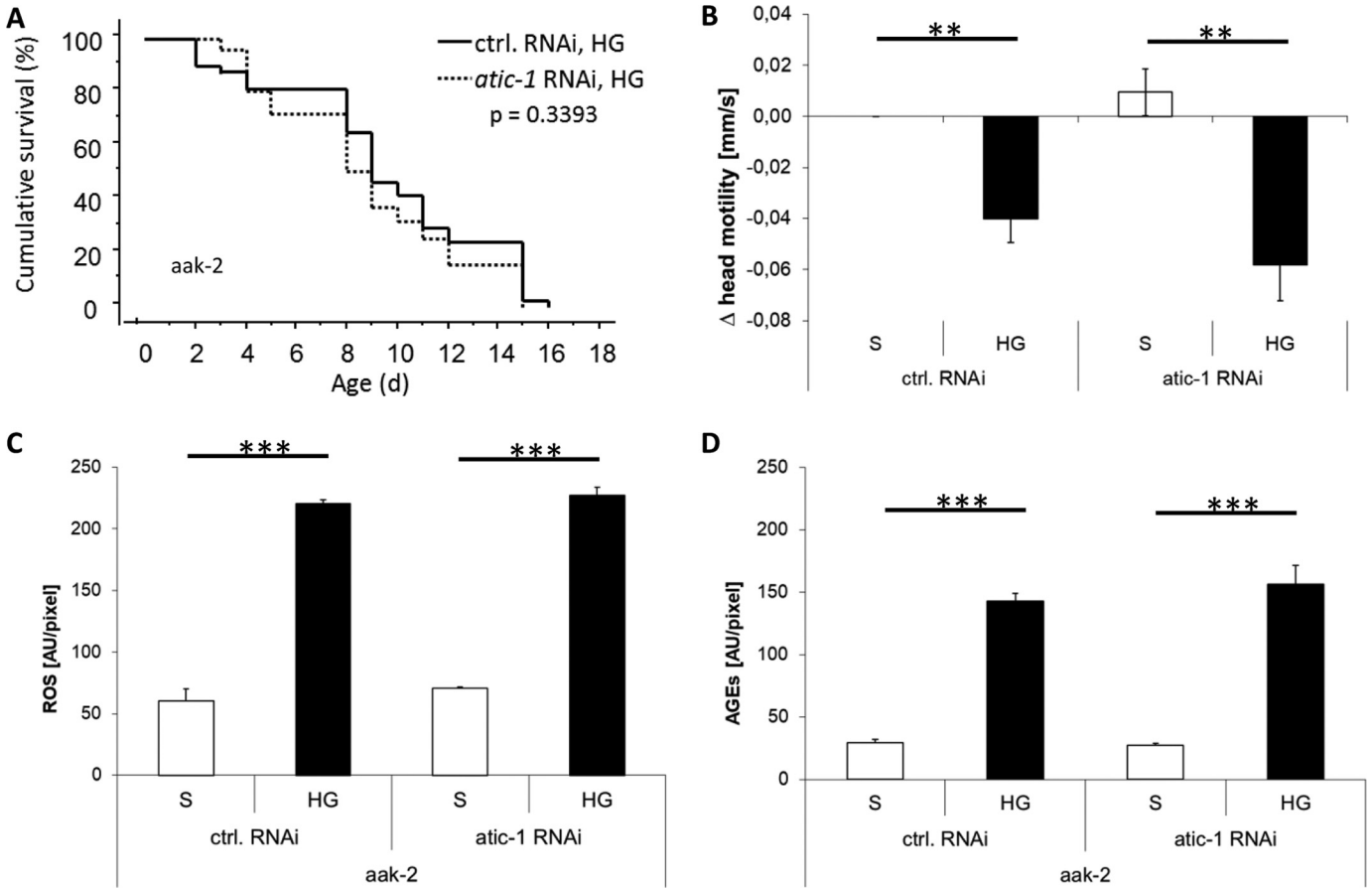

Figure 5. Effect of *atic-1* down-regulation on lifespan, neuronal damage, and reactive metabolites in *C. elegans* in an AMPK-dependent manner. *A*, effect of *atic-1* down-regulation on the lifespan of crtl (*solid line*) or *atic-1* RNAi (*dashed line*) feeding plates under HG conditions. One representative experiment of three independent experiments is shown, each with 60 nematodes per group. *d*, day. *B*, head motility was determined by video analysis as described under "Experimental procedures" under control or *atic-1* RNAi, each under S and HG conditions. Data represent mean ± S.D. of three independent experiments, each with 15 nematodes per group. *C*, ROS formation was detected by confocal laser-scanning microscopy of ethidium-labeled *C. elegans* as described under "Experimental procedures" under S and HG conditions. Data represent mean ± S.D. of three independent experiments, each with 20 nematodes per group. *D*, MG-derived AGE accumulation was detected by immunostaining and quantified by calculation of mean pixel values, as described under "Experimental procedures." Data represent mean ± S.D. of three independent experiments, each with 20 nematodes per group. **, $p < 0.01$; ***, $p < 0.001$; calculated using unpaired Student's *t* test.

formation of ds-breaks under S and HG conditions (Fig. 6), suggesting that there is no effect on purine synthesis. Thus, the effects of AICAR on all parameter studied were *aak-2* dependent. Furthermore, as the effect of AICAR treatment on all parameters studied was independent of *glod-4* and *sod-3*, mitochondrial targeting by AICAR was studied to better understand the mechanism underlying the effect of AICAR.

The effect of AICAR is independent of antioxidant defense pathways

HG-mediated lifespan reduction in WT nematodes (Fig. S7*A*, *first group*) was inhibited by AICAR as well as rotenone. However, co-administration of AICAR plus rotenone did not affect the lifespan, even under HG conditions. Thus, rotenone alone can substitute for AICAR under HG conditions. It is likely that the rotenone effect is distal from AICAR-mediated AMPK activation because, in the absence of *aak-2* (Fig. S7*A*, *second group*), the protective effect of AICAR was lost, whereas the effect of rotenone was not abrogated. Nevertheless, the effect of rotenone, as was the case with AICAR, was independent of the two major detoxifying enzymes *glod-4* (Fig. S7*A*, *third group*) and *sod-3* (Fig. S7*A*, *fourth group*). The hypothesis that the AICAR- and AMPK-dependent effect on lifespan was mediated by mitochondrial ROS production (and not detoxification) was supported by the effect of the antioxidant BHA, which prolonged the lifespan of the WT (Fig. S7*B*, *first group*) and could even, in the absence of *aak-2* (Fig. S7*B*, *second group*), prolong the lifespan, which was also independent of *glod-4* (Fig. S7*B*, *third group*) and *sod-3* (Fig. S7*B*, *fourth group*). The life-prolonging effect of AICAR was independent of *glod-4* ($p = 0.492$) and *sod-3* ($p = 0.274$) but dependent on *aak-2* ($p = 0{,}040$) (Fig. 7*A*). Further, the lifespan-prolonging effect of rotenone was independent of *aak-2* ($p = 0.254$), *glod-4* ($p = 0.390$), and *sod-3* ($p = 0.276$) (Fig. 7*B*). Further treatment of AICAR-treated nematodes with rotenone had no effect on the lifespan and was independent of *aak-2* ($p = 0.276$), *glod-4* ($p = 0.291$), and *sod-3* ($p = 0.237$) (Fig. 7*C*). The effect of BHA was independent of *aak-2* ($p = 0.299$), *glod-4* ($p = 0.118$), and *sod-3* ($p = 0.334$) (Fig. 7*D*). Combined treatment with AICAR and BHA did not improve the lifespan further and

was independent of *aak-2* ($p = 0.067$), *glod-4* ($p = 0.230$), and *sod-3* ($p = 0.174$) (Fig. 7*E*). It is important to note that the effects of rotenone and BHA were exclusively present in HG-treated nematodes, indicating that not basal mitohormesis-enabling ROS but, rather, HG-induced excessive ROS production is responsible for the HG effects observed.

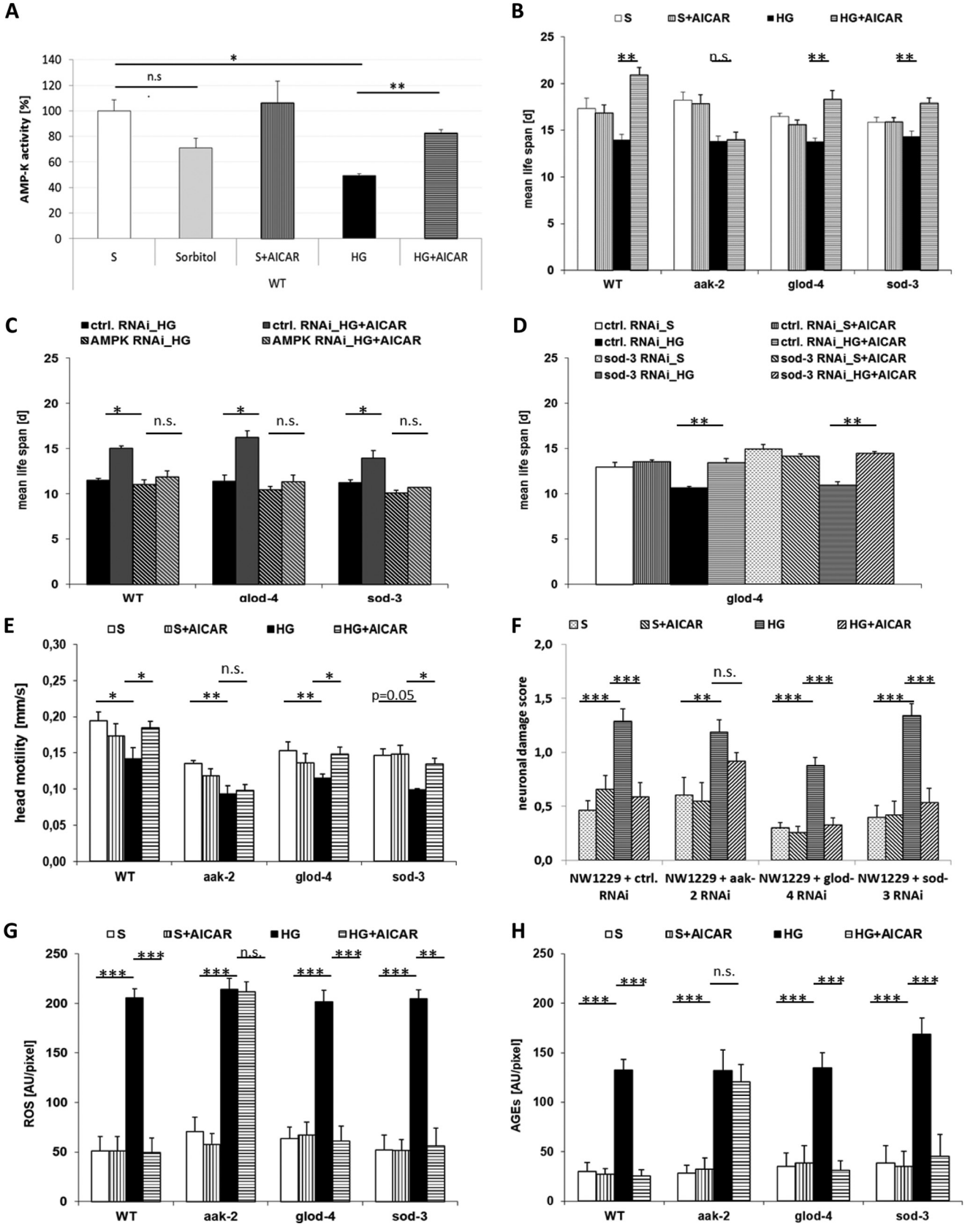

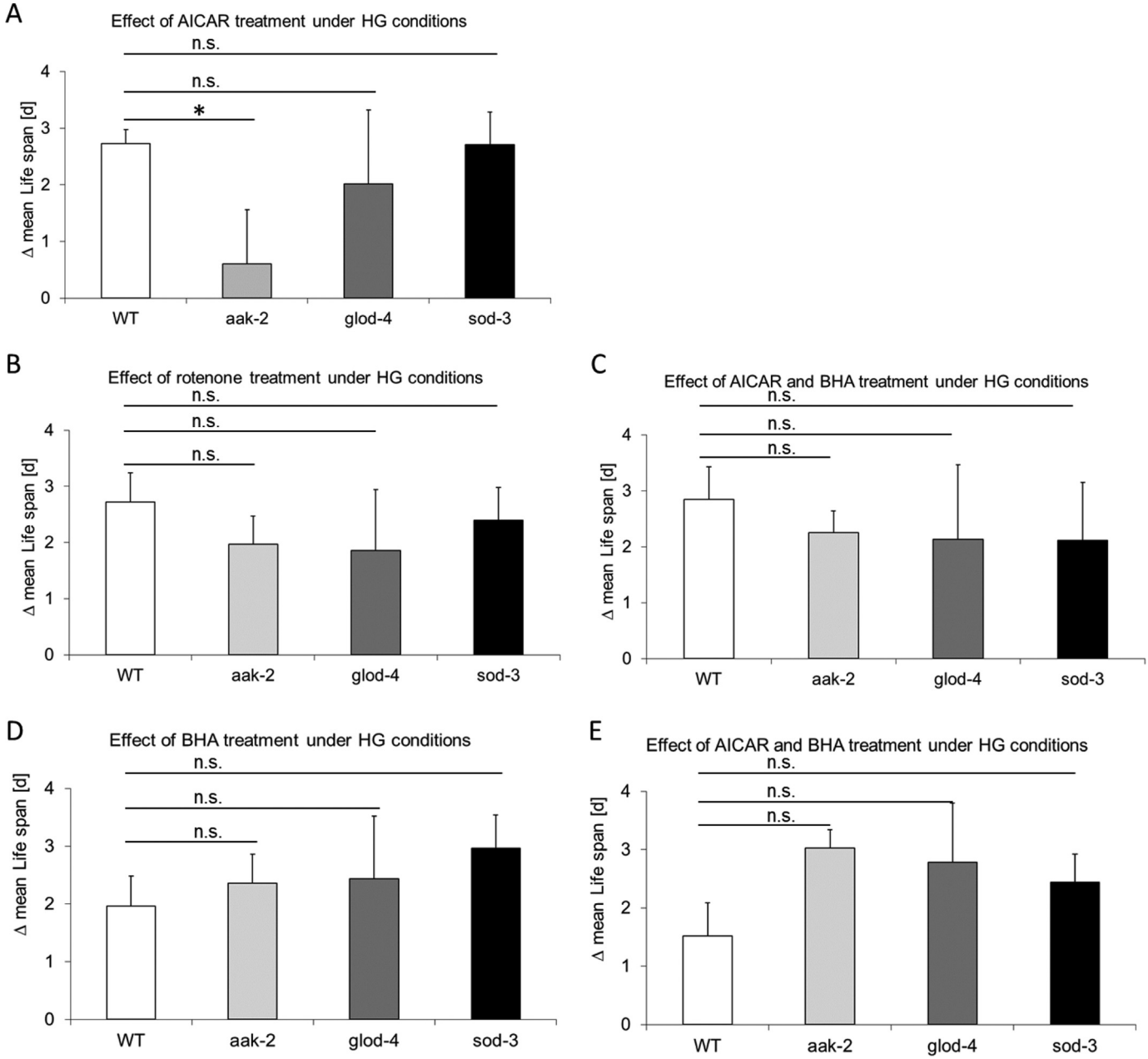

Figure 7. The effects of AICAR, BHA, and rotenone under HG conditions were dependent on AMPK and independent of glyoxalase-1 and superoxide dismutase-3. *A–C*, effect of treatment with 100 nM rotenone (a complex 1 inhibitor) on the lifespan of AICAR-treated nematodes under HG conditions in WT and *aak-2*-, *glod-4*-, and *sod-3*-deficient nematodes. *D* and *E*, effect of treatment with 25 μM BHA (an antioxidant) on the lifespan of AICAR-treated nematodes under HG conditions. Data represent mean ± S.D. of three independent experiments, each with 60 nematodes per group. *, $p < 0.05$, calculated using unpaired Student's *t* test. *n.s.*, not significant.

Figure 6. The Effect of AICAR under HG conditions is dependent on AMPK and independent of glyoxalase-1 and superoxide dismutase-3. *C. elegans* were cultivated under S and HG conditions and treated with 1 mM AICAR. *A*, effect of HG and AICAR on AMPK activity over time and effect of HG and AICAR (1 mM) treatment on AMPK activity under S and HG conditions in WT nematodes after 5-day treatment. Data represent mean ± S.D., each with 1000 nematodes per group. *B*, effect of AICAR on the lifespan of different mutant nematodes as indicated. Data represent mean ± S.D. of three independent experiments, each with 60 nematodes per group. *C*, lifespan of *C. elegans* grown on ctrl RNAi and *aak-2* RNAi feeding plates under HG conditions. Data represent mean ± S.D. of three independent experiments, each with 60 nematodes per group. *D*, lifespan of *glod-4 C. elegans* grown on ctrl and *sod-3* RNAi feeding plates under S and HG conditions. Shown are means and standard errors of three independent experiments, each with 60 nematodes per group. *E*, head mobility was determined by video analysis as described under "Experimental Procedures" under S and HG conditions. Data represent mean ± S.D. of three independent experiments, each with 20 nematodes per group. *F*, neuronal structure was visualized by a pan-neuronal-specific GFP reporter, and neuronal damage was scored in a blinded procedure as described under "Experimental Procedures" under S or HG conditions (NW1229: WT nematodes carrying a pan-neuronal-specific GFP reporter). Data represent mean ± S.D. of three independent experiments, each with 20 nematodes per group. *G*, ROS formation was detected by confocal laser-scanning microscopy of ethidium-labeled *C. elegans* as described under "Experimental Procedures," cultivated under S and HG conditions. Data represent mean ± S.D. of three independent experiments, each with 20 nematodes per group. *H*, MG-derived AGEs accumulation was detected by immunostaining, and the mean pixel intensity was quantified as described under "Experimental Procedures." Data represent mean ± S.D. of three independent experiments, each with 20 nematodes per group. *, $p < 0.05$; **, $p < 0.01$; ***, $p < 0.001$; calculated using unpaired Student's *t* test. *n.s.*, not significant.

Discussion

This study identified C55F2.1 as the *C. elegans* homolog for the mammalian enzyme ATIC. In contrast to mice and humans (27, 28), where HG is associated with increased genomic DNA damage, especially DNA double strand breaks but also interchain cross-links and DNA–protein cross-links (17), there was no evidence of genomic DNA damage being significantly associated with the glucose effects in the model under HG conditions studied. Thus, the HG induced up-regulation of *atic-1* is not needed for improving DNA repair in response to HG, and a possible physiological benefit of an *atic-1* overexpression remains unknown. However, only genomic DNA damage was studied, which, in the nematode, is dependent on the RecA homolog (29), which does not exclude that mitochondrial DNA damage might play a role in HG-mediated complications, too. Previous studies have shown, in *C. elegans*, that reactive metabolites preliminarily target mitochondrial proteins (30–34) and that mitochondrial DNA repair involving *exo-3* is important in the regulation response to increased production of reactive metabolites (19). Future studies are needed to address the role of mitochondrial DNA damage and repair in the HG-exposed nematode.

Nevertheless, inhibiting *atic-1* expression resulted, under HG conditions, in unchanged development of DNA double strand breaks compared with S conditions and an increase of ds-breaks compared with ctrl RNAi conditions. This indicates that, even in the nematode, not only the RecA homolog (29) but also purine synthesis is important. Under HG conditions, baseline purine synthesis is sufficient to ensure baseline DNA repair.

The findings of this study are more consistent with an important role of the ATIC–AICAR pathway in AMPK regulation of mitochondrial dysfunction, resulting in the generation of reactive metabolites and a subsequent increase in neuronal dysfunction and/or damage and reduction of the lifespan. This is supported by three lines of evidence. First, the effect of *atic-1* inhibition and the effect of AICAR administration were entirely dependent on the action of *aak-2* and independent of the classical ROS-scavenging and MG-detoxifying activities of *sod-3* and *glod-4*. Second, rotenone, targeting mitochondrial complex I, could normalize the lifespan (35) independent of *aak-2*, *sod-3*, and *glod-4*. Thus it could be hypothesized that AICAR/AMPK normalizes mitochondrial dysfunction in the presence of HG because AICAR addition could not improve the lifespan in the presence of rotenone. Third, the antioxidant BHA also improved the effects of HG-induced events. In the presence of BHA, neither AICAR nor *aak-2*, *sod-3*, or *glod-4* were required for defense against the HG effects.

These findings would suggest that rotenone is able to reduce mitochondrial superoxide formation, protecting against the effects of HG-induced metabolite accumulation and neuronal damage. This is in contrast to a study in mice that showed that mitochondrial ROS formation inhibited AMPK and reduced streptozotocin diabetes-induced renal damage (9). A possible explanation for this difference could be the very fine hometic ROS response in different organisms (11). Although a certain dose of ROS might be protective in one model system, it might be detrimental in another (14). This holds true in *C. elegans* because the protective ROS signal requires *aak-2* (36, 37). A potential master regulator for this might be *daf-2*, which also regulates AMPK (38), consistent with the concept of mitohormesis causing an adaptive, life-prolonging effect involving crosstalk with L-proline metabolism (37). Future studies are required to determine the relative contribution of this cross-talk to the protective effect observed.

Such cross-talk would also affect the complex cell– cell interactions that occur in protecting against the effects of HG. Down-regulation of *atic-1* by RNAi treatment resulted in protection of head motility and structural neuronal damage despite the fact that RNAi treatment does not reach neuronal cells, as shown previously by others and in our model system (39, 40). Thus, non-neuronal cells affected by RNAi could send sufficient warning signals to neuronal cells to prepare to defend themselves against glucotoxic effects. Alternatively, HG could change the function of non-neuronal cells, which, after having acquired a dysfunctional phenotype, send signals to neuronal cells, leading to their damage. Future studies would be required to distinguish between these two possibilities and determine the cell type responsible for the RNAi effects that have been described.

The induction of *atic-1* by HG did not result in depletion of AICAR. The physiological capacity of *atic-1* in *C. elegans* seems to be sufficient to ensure purine synthesis, and the basal concentration of AICAR was not affected by HG. In addition, the physiological concentration of AICAR measured in the nematodes was at the lower detection limit and far below the AICAR concentrations needed to pharmacologically induce AMPK activity (41). Nevertheless, even though not important for the system studied here, down-regulation of *atic-1* increased AICAR, consistent with a constant basal turnover of AICAR by *atic-1* and the defense against HG seen when pharmacological doses of AICAR were used. This subsequently resulted in a reduction of ROS (21), MG-dependent AGEs, and neuronal dysfunction. It remains unknown whether the AICAR-mediated effects of *atic-1* down-regulation are targeting mitochondrial complex I alone or whether the AICAR-mediated reduction of *atic-1* mRNA expression is also involved. However, it can be concluded that the major effect of the ATIC–AICAR pathway is toward the correction of mitochondrial dysfunction. Interestingly, loss of *sod-3* or *glod-4* did not impair the ATIC–AICAR effect in this setting, compatible with a model of protection against ROS and dicarbonyls not on the level of detoxification but, rather, by addressing the mitochondrial dysfunction– dependent generation of these metabolites.

Experimental procedures

Cloning and bacterial overexpression of atic-1

The ATIC homologue C55F2.1b was cloned using cDNA of wildtype *C. elegans* (RNeasy Micro Kit, Qiagen, Hilden, Germany; First Strand cDNA Synthesis Kit for RT-PCR, Roche Diagnostics, Mannheim, Germany) with primers carrying a

BamHI and KpnI restriction site, respectively (forward primer, 5′-CGA GGA TCC TGA AAT GAC CGA CGG AAA ATC AC-3′; reverse primer, 5′- AAA GGT ACC GTG TGG AAG AGA CGA AGT CCA GT-3′). The 1955-bp fragment was then ligated in-frame into the vector pVH10.05 (kindly provided by H. Hutter) between the neuronal F25.B.3 promotor and the GFP-tag for neuronal overexpression. For ubiquitous overexpression, the ribosomal promotor Prps-5 was cloned via PstI/BamHI from the vector L4453 (kindly provided by Andrew Fire, Addgene plasmid 1655) into the plasmid pPB95.85 (Andrew Fire, Addgene plasmid 1498). In a second step, the PCR product was ligated in-frame into the vector between the ribosomal promotor and the GFP tag via BamHI/KpnI. Restriction enzymes and ligase were used following the manufacturer's instructions (New England Biolabs, Frankfurt, Germany). Before further using the plasmids, the sequence was confirmed by DNA sequencing.

Generation of transgenic C. elegans by microinjection and genomic integration

The plasmids pPB95.85+*atic-1* (Prps-5:: C55F2.1b::GFP) and pVH10.05+ *atic-1* (F25.B3.3:: C55F2.1b::YFP) were co-injected into the gonads of adult *pha-1* hermaphrodites together with pBX carrying wild-type *pha-1* (42, 43). 2–3 μl was injected with a micromanipulator (LN Mini 25, Luigs und Neumann, Ratingen, Germany) in each worm (50 ng/ml *pha-1* + 50 ng/ml of the gene of interest in Tris (pH 7.5)) with a freshly pulled injection needle (model P-97, Sutter Instruments, Novato, CA) (42, 44). The injected nematodes were then cultivated at 25 °C to select for *pha-1*–positive individuals. Two independent strains were obtained for ubiquitous *atic-1* expression (VH2190, *pha-1*(e2123) hdEx574(Prps-5:: C55F2.1b::GFP;*pha-1*(+)) and VH2191, *pha-1*(e2123) hdEx575(Prps-5:: C55F2.1b::GFP;*pha-1*(+))) and two strains for nuclear overexpression (VH2199, *pha-1*(e2123) hdEx576 (F25.B3.3:: C55F2.1b::GFP;*pha-1*(+)) and VH2202: *pha-1*(e2123) hdEx577 (F25.B3.3:: C55F2.1b::GFP;*pha-1*(+))). Further experiments with extrachromosomal strains were performed at 25 °C to maintain the selection pressure.

Genomic integration was achieved by UV treatment. Freshly starved nematodes containing ideally about 50% transgenic nematodes were transferred to fresh plates and incubated at 25 °C. After 1–2 days, the plates were UV-exposed (UV Crosslinker FB-UVXL-1000, Fisher Scientific, 300 J/m^2). After 1 h of rest, healthy-looking L4 larvae were transferred to fresh plates, four to five worms per plate, and starved at 15 °C. To isolate the expected F2-generation for each strain, 600 nematodes were isolated and cultivated at 15 °C. Plates with 100% positive fluorescence were selected, and the homozygous animals were outcrossed three times with wildtype nematodes (N2) (CGC, Minneapolis, MN). VH2199 could be successfully integrated to achieve the strain VH2202:Is (F25.B3.3:: C55F2.1b::GFP;*pha-1*(+)).

C. elegans maintenance

The wildtype (N2 Bristol), the *sod-3* mutant strain VC433 (*sod-3*(*gk235*)X.), the AMPK knockout mutant strain RB754 (*aak-2*(*ok524*)X), the *glo-1* mutant strain VC343 (*glod-4*(*gk189*)III.) and the pan-neuronal GFP-expressing strain NW1229 (*Prgef-1::GFP(evIs111)*) (45) were kindly provided by the *Caenorhabditis* Genetics Center (University of Minnesota, Minneapolis, MN).

C. elegans were cultured on 60-mm nematode growth medium plates on an OP50 lawn (*Caenorhabditis* Genetics Center, University of Minnesota) and transferred to 5-fluorodesoxyuridine plates (300 μg/ml 5-fluorodesoxyuridine, Sigma-Aldrich, Taufkirchen, Germany) on day 1 of adulthood for the respective experiments. The feeding method was used for the evaluation of RNAi-treatment (I/C plates; nematode growth medium plus 1 mM isopropyl-β-D-1-thiogalactopyranoside and 25 μg/ml carbenicillin) with *Escherichia coli* HT115-expressing RNAi for *aak-2*, *atic-1*, *glod-4*, *sod-3*, or control RNAi, respectively (provided by the Fire Lab *C. elegans* vector kit (principal investigator Andrew Fire, Addgene, Cambridge, MA)). The nematodes were transferred to new plates daily in the RNAi experiments.

For high glucose stimulation, the worms were treated daily with 150 μl of a 400 mmol/liter glucose solution for 5 days. One hundred fifty microliters of 400 mmol/liter glucose solution achieved an intracellular glucose concentration of 14 mmol/liter in the nematode (31).

Determination of lifespan

In lifespan assays, the nematodes were cultivated on 5-fluorodesoxyuridine or I/C plates under S or HG conditions (30), leading to glucose concentrations of 5.5 mmol/liter (99 mg/dl) and 13 mmol/liter (234 mg/dl) in whole-worm extracts, respectively (31). Where indicated, 150 μl of AICAR, BHA, and rotenone were added at a concentration of 1 mM AICAR, 25 μM BHA, and 100 nM rotenone, respectively. The nematodes were regarded as dead when they did not move after repeated stimuli. Animals were excluded when they crawled away from the plate, crept into the agar, or contained internally hatched larvae. Experiments were performed at least in triplicates with 60 animals each.

The lifespan experiments with tgATIC mutant nematodes (VH2190) were performed at 15 °C to exclude *pha-1*–dependent effects. Nematodes without fluorescence were used as controls. The experiments with the GFP-expressing strain NW1229 were performed at 25 °C to maintain the selected pressure. All other experiments were performed at 20 °C.

Quantification of gene expression

mRNA was isolated (RNeasy Micro Kit, Qiagen) and transcribed to cDNA (First Strand cDNA Synthesis Kit for RT-PCR, Roche Diagnostics), followed by quantitative real-time PCR by the second derivate maximum method (Lightcycler, Roche Diagnostics). Primers were used as follows (Thermo Electron, Ulm, Germany): *atic-1*, 5′-GGA AGA GAC GAA GTC CAG TAT GA-3′ and 5′-CAG CAA ACA GGA GTT GTF ATG AG-3′; *tbg-1* (reference sequence), 5′-TGA TGA CTG TCC ACG TTG GA-3′ and 5′-CGT CAT CAG CCT GGT AGA ACA-3′ (46).

Evaluation of neuronal damage

Structural damage was determined using a semiquantitative four-staged classification scheme in a blinded procedure (47). The pan-neuronal GFP-expressing strain NW1229 (45)

and the pan-neuronal *atic-1*::GFP fusion protein overexpressing strain VH2202 were visualized by fluorescence microscopy. At least 20 nematodes were scored (0: healthy, no damage; 1: minor damage; 2: major damage; 3: extended loss of neuronal structure and dead animals, these were excluded). To assess head motility as a functional parameter, video analysis was performed at day 12 of adulthood (Moticam 1000, Beyersdörfer, Mandelbachtal, Germany). Relative head motility was calculated with a worm tracking software (WormTracker 4.0, Thomas Bornhaupt, Neustadt/Weinstraße).

Quantification of ROS and MG-derived AGEs

ROS were detected by oxidation of the O_2-sensitive hydroethidine to ethidium (48). MG-derived AGEs were detected by immunostaining with a mouse primary antibody (AGE06B, Biologo, Kronshagen, Germany) and visualized by an Alexa Fluor–labeled goat secondary antibody (Invitrogen, A11002, Thermo Fisher, Rockford, IL). ROS and MG-derived AGEs were quantified by confocal laser-scanning microscopy (30) and calculated by mean pixel intensities with ImageJ software (49). ROS measurement by quantification of H_2O_2 concentration was shown to give similar results before (48).

Quantification of DNA damage

DNA damage was determined by alkaline comet assay (50). Nematodes were treated with HBSS buffer (1× Hanks' balanced salt solution (Sigma-Aldrich), 20 nM EDTA, and 10% DMSO (pH 8)) and triturated with a glass pistil to isolate the *C. elegans* cells. The isolated cells were mixed with low-melting-point agarose, and the mixture was loaded on an agar-coated microscope slide. The slides were immersed in ice-cold lysis solution (2.3 M NaCl, 100 mM EDTA, 10 mM Trizma base, 1% Triton X-100, and 10% DMSO) at 4 °C for 3 h. Electrophoresis was performed for 25 min at 24 V in electrophoresis buffer (33 mM NaoH and 200 mM EDTA). After electrophoresis, the slides were washed with neutralization buffer (0.4 M Tris) and stained with 4′,6-diamidino-2-phenylindole (1 μg/ml). Quantification (51–53) was performed with a fluorescence microscope.

Determination of AICAR levels in C. elegans

AICAR was determined in whole-worm extracts. A pellet with ~800 nematodes was homogenized in M9 medium (22 mM KH_2PO_4, 42 mM Na_2HPO_4, and 86 mM NaCl (pH 7)) by using a Bullet Blender Blue (Next Advance, Inc., Burden Lake Road, NY). Protein concentration was determined by using bovine serum albumin as standard. Before analysis, the samples were diluted with distilled water to a total protein concentration of 1 mg/ml. To a 180-μl aliquot of diluted *C. elegans* was added 20 μl of 50 μM Thymin-d4 internal standard (Cambridge Isotopes, Tewksbury, MA); this was filtrated with a centrifuge filter (Merck Millipore, Darmstadt, Germany) with a pore size of 0.1 μm. On a Quattro Ultima triple quadrupole mass spectrometer (Micromass, Manchester, UK) equipped with an electrospray ion source and a Micromass MassLynx data system (according to Hartmann *et al.* (54) with some modifications and the admission of AICAR), we performed liquid chromatography. The optimized multiple reaction monitoring experiment was performed on the most abundant ion transition (*m/z* 259 – 127), which was identified by direct infusion of AICAR (Sigma-Aldrich). Argon as collision gas (collision with an energy of 14 electron volt) was operated in positive ion mode with a needle voltage of 3.15 kV. The system was equipped with a C18 2.0 × 4 mm precolumn cartridge (Phenomenex, Aschaffenburg, Germany) and a Phenomenex Aqua C18 column (2.0 × 250 mm, 5-μm particle size). The chromatographic run was performed at 100 μl/min with a gradient profile between 0.05 M acetic acid (pH 2.8) (eluent A) and 0.05 M acetic acid (pH 2.8) and methanol (1:1, v/v) (eluent B). The gradient started at 100% A, held isocratic for 2.0 min, increased to 100% B over 8 min, switched to 100% A over 1.5 min, and re-equilibrated for 8.5 min at 100% A. 20 min was the overall run time, and 20 μl was the injection volume. Concentrations were calculated by signal AICAR toward AICAR signal into internal standard signal and a four-point calibration curve (0 – 0.5 μM).

Determination of AMPK activity

AMPK activity was determined in whole-worm extracts by an AMPK activity assay (catalog no. CY-1182, CycLex) (55). A pellet with ~1000 nematodes was homogenized in lysis medium (50 mM HEPES, 50 mM KCl, 1 mM EDTA, 1 mM EGTA, 5 mM β-glycerol phosphate, protease inhibitor mixture (Complete, Roche), 50 mM NaF, 1 mM sodium orthovanadate, 5 mM sodium pyrophosphate, and 0.2 mM phenylmethylsulfonyl fluoride) by using a Bullet Blender Blue (Next Advance, Inc.). Protein concentration was determined by using bovine serum albumin as standard. A 10-μl sample was mixed with 90 μl of kinase reaction buffer (50 μM ATP) and incubated at 37 °C for 45 min. The wells were washed five times with wash buffer. 100 μl of anti-phospho-mouse monoclonal antibody was pipetted into the wells and incubated for 30 min at room temperature. The wells were washed five times, 100 μl of substrate reagent was added, and then this was incubated for 15 min at room temperature. Then we added 100 μl of stop solution to the well and measured absorbance at 450 nm.

Determination of AICAR formyltransferase activity

AICARFT was determined by initial appearance of tetrahydrofolate at 298 nm as described by Black *et al.* (56), employing a thermostatic spectrometer. The cuvette contained 32.5 μM Tris-HCl (pH 7), 5 μM β-mercaptoethanol, 25 μM KCl, 0.101 μM 10-formyl-tetrahydrofolate, and enzyme; it was filled up to 0.950 ml under N_2 at 25 °C. First the non-enzymatic rate was recorded for 10 min and later abstracted from the initial rate obtained after adding 0.05 ml of 1.01 mM AICAR. All educts were prepared from degassed H_2O and were N_2-saturated because the blank rate was very sensitive to the amount of oxygen in the solutions. The reaction mixture for the recombinant C55F2.1 protein was mixed prior to the addition of the human AICARFT/IMPCHase (IMP cyclohydroxylase) enzyme and subsequently mixed again.

Determination of methylglyoxal production

MG concentration was measured in whole *C. elegans* lysate as described by Tötemeyer *et al.* (57). The lysate was prepared by using a Bullet Blender Blue (Next Advance, Inc.), transferred to tubes, and stored at −20 °C until the assay was performed. MG was assayed colorimetrically using 2,4-dinitrophenolhydrazine. In the assay, standard (10 μl containing 0–10 nM MG) and sample were added to the wells, and then 70 μl of distilled water plus 30 μl of 0.1% 2,4-dinitrophenolhydrazine in 2 M HCl was added. After 15 min at room temperature, 140 μl of 10% NaOH was added. After a further incubation of 10 min at room temperature, the absorbance was measured at 540 nm. The recombinant ATIC protein (Abnova, Neihu, Taiwan) was mixed with 1 mM dihydroxyacetone phosphate in 50 mM imidazole-HCl (pH 7) and incubated for 30 min at 30 °C to produce MG.

Statistical analyses

Statistical analyses were performed with Excel 2010 (Microsoft, Redmond, WA) and StatView 5.0 (SAS Institute, Cary, NC). The difference between two groups was analyzed by unpaired Student's t test, and $p < 0.05$ was considered to be significant, $p < 0.01$ highly significant, and $p < 0.001$ extremely highly significant. Analysis of variance was used for comparisons of multiple groups, and Fisher's protected least significant difference *post hoc* tests were used for additional between-group comparisons.

Author contributions—C. R., M. M., and A. S. performed experiments and analyzed data. C. R., M. M., T. F., and P. P. N. designed the studies. C. R., M. M., T. F., J. O., H.-P. H., S. H., and P. P. N. wrote the manuscript and discussed it. All authors reviewed the results and approved the final version of the manuscript.

Acknowledgments—We thank Dr. Harald Hutter (Simon Fraser University, Department of Biological Sciences, Canada) for support and for teaching us how to create transgenic nematodes and the Fire Lab (Departments of Pathology and Genetics, Stanford University School of Medicine) for creating the plasmids. We also thank Kathrin Schmidt for excellent technical assistance.

References

1. Corton, J. M., Gillespie, J. G., Hawley, S. A., and Hardie, D. G. (1995) 5-Aminoimidazole-4-carboxamide ribonucleoside: a specific method for activating AMP-activated protein kinase in intact cells? *Eur. J. Biochem.* **229,** 558–565 CrossRef Medline
2. Hawley, S. A., Selbert, M. A., Goldstein, E. G., Edelman, A. M., Carling, D., and Hardie, D. G. (1995) 5′-AMP activates the AMP-activated protein kinase cascade, and Ca2+/calmodulin activates the calmodulin-dependent protein kinase I cascade, via three independent mechanisms. *J. Biol. Chem.* **270,** 27186–27191 CrossRef Medline
3. Davies, S. P., Helps, N. R., Cohen, P. T., and Hardie, D. G. (1995) 5′-AMP inhibits dephosphorylation, as well as promoting phosphorylation, of the AMP-activated protein kinase: studies using bacterially expressed human protein phosphatase-2C α and native bovine protein phosphatase-2AC. *FEBS Lett.* **377,** 421–425 CrossRef Medline
4. Suter, M., Riek, U., Tuerk, R., Schlattner, U., Wallimann, T., and Neumann, D. (2006) Dissecting the role of 5′-AMP for allosteric stimulation, activation, and deactivation of AMP-activated protein kinase. *J. Biol. Chem.* **281,** 32207–32216 CrossRef Medline
5. Song, X. M., Fiedler, M., Galuska, D., Ryder, J. W., Fernström, M., Chibalin, A. V., Wallberg-Henriksson, H., and Zierath, J. R. (2002) 5-Aminoimidazole-4-carboxamide ribonucleoside treatment improves glucose homeostasis in insulin-resistant diabetic (ob/ob) mice. *Diabetologia* **45,** 56–65 CrossRef Medline
6. Bergeron, R., Previs, S. F., Cline, G. W., Perret, P., Russell, R. R., 3rd, Young, L. H., and Shulman, G. I. (2001) Effect of 5-aminoimidazole-4-carboxamide-1-β-D-ribofuranoside infusion on *in vivo* glucose and lipid metabolism in lean and obese Zucker rats. *Diabetes* **50,** 1076–1082 CrossRef Medline
7. Buhl, E. S., Jessen, N., Schmitz, O., Pedersen, S. B., Pedersen, O., Holman, G. D., and Lund, S. (2001) Chronic treatment with 5-aminoimidazole-4-carboxamide-1-β-D-ribofuranoside increases insulin-stimulated glucose uptake and GLUT4 translocation in rat skeletal muscles in a fiber type-specific manner. *Diabetes* **50,** 12–17 CrossRef Medline
8. Iglesias, M. A., Ye, J. M., Frangioudakis, G., Saha, A. K., Tomas, E., Ruderman, N. B., Cooney, G. J., and Kraegen, E. W. (2002) AICAR administration causes an apparent enhancement of muscle and liver insulin action in insulin-resistant high-fat-fed rats. *Diabetes* **51,** 2886–2894 CrossRef Medline
9. Dugan, L. L., You, Y. H., Ali, S. S., Diamond-Stanic, M., Miyamoto, S., DeCleves, A. E., Andreyev, A., Quach, T., Ly, S., Shekhtman, G., Nguyen, W., Chepetan, A., Le, T. P., Wang, L., Xu, M., *et al.* (2013) AMPK dysregulation promotes diabetes-related reduction of superoxide and mitochondrial function. *J. Clin. Invest.* **123,** 4888–4899 CrossRef Medline
10. Ruderman, N. B., Carling, D., Prentki, M., and Cacicedo, J. M. (2013) AMPK, insulin resistance, and the metabolic syndrome. *J. Clin. Invest.* **123,** 2764–2772 CrossRef Medline
11. Ristow, M., and Schmeisser, K. (2014) Mitohormesis: promoting health and lifespan by increased levels of reactive oxygen species (ROS). *Dose Response* **12,** 288–341 Medline
12. Onken, B., and Driscoll, M. (2010) Metformin induces a dietary restriction-like state and the oxidative stress response to extend *C. elegans* healthspan via AMPK, LKB1, and SKN-1. *PLoS ONE* **5,** e8758 CrossRef Medline
13. Schlernitzauer, A., Oiry, C., Hamad, R., Galas, S., Cortade, F., Chabi, B., Casas, F., Pessemesse, L., Fouret, G., Feillet-Coudray, C., Cros, G., Cabello, G., Magous, R., and Wrutniak-Cabello, C. (2013) Chicoric acid is an antioxidant molecule that stimulates AMP kinase pathway in L6 myotubes and extends lifespan in *Caenorhabditis elegans*. *PLoS ONE* **8,** e78788 CrossRef Medline
14. Ristow, M., and Schmeisser, S. (2011) Extending life span by increasing oxidative stress. *Free Radic. Biol. Med.* **51,** 327–336 CrossRef Medline
15. Mungai, P. T., Waypa, G. B., Jairaman, A., Prakriya, M., Dokic, D., Ball, M. K., and Schumacker, P. T. (2011) Hypoxia triggers AMPK activation through reactive oxygen species-mediated activation of calcium release-activated calcium channels. *Mol. Cell Biol.* **31,** 3531–3545 CrossRef Medline
16. Kukidome, D., Nishikawa, T., Sonoda, K., Imoto, K., Fujisawa, K., Yano, M., Motoshima, H., Taguchi, T., Matsumura, T., and Araki, E. (2006) Activation of AMP-activated protein kinase reduces hyperglycemia-induced mitochondrial reactive oxygen species production and promotes mitochondrial biogenesis in human umbilical vein endothelial cells. *Diabetes* **55,** 120–127 CrossRef Medline
17. Xavier, D. J., Takahashi, P., Evangelista, A. F., Foss-Freitas, M. C., Foss, M. C., Donadi, E. A., Passos, G. A., and Sakamoto-Hojo, E. T. (2015) Assessment of DNA damage and mRNA/miRNA transcriptional expression profiles in hyperglycemic versus non-hyperglycemic patients with type 2 diabetes mellitus. *Mutat. Res.* **776,** 98–110 CrossRef Medline
18. Kasznicki, J., Krupa, R., Błasiak, J., and Drzewoski, J. (2009) Association between polymorphisms of the DNA repair genes XRCC1 and hOGG1 and type 2 diabetes mellitus in the Polish population. *Pol. Arch. Med. Wewn.* **119,** 122–128 Medline
19. Schlotterer, A., Hamann, A., Kukudov, G., Ibrahim, Y., Heckmann, B., Bozorgmehr, F., Pfeiffer, M., Hutter, H., Stern, D., Du, X., Brownlee, M., Bierhaus, A., Nawroth, P., and Morcos, M. (2010) Apurinic/apyrimidinic

endonuclease 1, p53, and thioredoxin are linked in control of aging in *C. elegans*. *Aging Cell* **9**, 420–432 CrossRef Medline
20. Vlassara, H., and Palace, M. R. (2002) Diabetes and advanced glycation endproducts. *J. Intern. Med.* **251,** 87–101 CrossRef Medline
21. Habib, S. L., Yadav, A., Kidane, D., Weiss, R. H., and Liang, S. (2016) Novel protective mechanism of reducing renal cell damage in diabetes: activation AMPK by AICAR increased NRF2/OGG1 proteins and reduced oxidative DNA damage. *Cell Cycle* **15,** 3048–3059 CrossRef Medline
22. Bhatt, S., Gupta, M. K., Khamaisi, M., Martinez, R., Gritsenko, M. A., Wagner, B. K., Guye, P., Busskamp, V., Shirakawa, J., Wu, G., Liew, C. W., Clauss, T. R., Valdez, I., El Ouaamari, A., Dirice, E., *et al.* (2015) Preserved DNA damage checkpoint pathway protects against complications in long-standing type 1 diabetes. *Cell Metab.* **22,** 239–252 CrossRef Medline
23. Tewari, S., Santos, J. M., and Kowluru, R. A. (2012) Damaged mitochondrial DNA replication system and the development of diabetic retinopathy. *Antioxid. Redox Signal.* **17,** 492–504 CrossRef Medline
24. Rani, V., Deep, G., Singh, R. K., Palle, K., and Yadav, U. C. (2016) Oxidative stress and metabolic disorders: pathogenesis and therapeutic strategies. *Life Sci.* **148,** 183–193 CrossRef Medline
25. Blasiak, J., Arabski, M., Krupa, R., Wozniak, K., Zadrozny, M., Kasznicki, J., Zurawska, M., and Drzewoski, J. (2004) DNA damage and repair in type 2 diabetes mellitus. *Mutat. Res.* **554,** 297–304 CrossRef Medline
26. Sliwinska, A., Blasiak, J., Kasznicki, J., and Drzewoski, J. (2008) *In vitro* effect of gliclazide on DNA damage and repair in patients with type 2 diabetes mellitus (T2DM). *Chem. Biol. Interact.* **173,** 159–165 CrossRef Medline
27. Ghiraldini, F. G., Crispim, A. C., and Mello, M. L. (2013) Effects of hyperglycemia and aging on nuclear sirtuins and DNA damage of mouse hepatocytes. *Mol. Biol. Cell* **24,** 2467–2476 CrossRef Medline
28. Tornovsky-Babeay, S., Dadon, D., Ziv, O., Tzipilevich, E., Kadosh, T., Schyr-Ben Haroush, R., Hija, A., Stolovich-Rain, M., Furth-Lavi, J., Granot, Z., Porat, S., Philipson, L. H., Herold, K. C., Bhatti, T. R., Stanley, C., *et al.* (2014) Type 2 diabetes and congenital hyperinsulinism cause DNA double-strand breaks and p53 activity in β cells. *Cell Metab.* **19,** 109–121 CrossRef Medline
29. O'Neil, N., and Rose, A. (2006) in *WormBook*, ed. The *C. elegans* Research Community, WormBook, 10.1895/wormbook.1.7.1
30. Morcos, M., Du, X., Pfisterer, F., Hutter, H., Sayed, A. A., Thornalley, P., Ahmed, N., Baynes, J., Thorpe, S., Kukudov, G., Schlotterer, A., Bozorgmehr, F., El Baki, R. A., Stern, D., Moehrlen, F., *et al.* (2008) Glyoxalase-1 prevents mitochondrial protein modification and enhances lifespan in *Caenorhabditis elegans*. *Aging Cell* **7**, 260–269 CrossRef Medline
31. Schlotterer, A., Kukudov, G., Bozorgmehr, F., Hutter, H., Du, X., Oikonomou, D., Ibrahim, Y., Pfisterer, F., Rabbani, N., Thornalley, P., Sayed, A., Fleming, T., Humpert, P., Schwenger, V., Zeier, M., *et al.* (2009) *C. elegans* as model for the study of high glucose- mediated life span reduction. *Diabetes* **58**, 2450–2456 CrossRef Medline
32. Bierhaus, A., Fleming, T., Stoyanov, S., Leffler, A., Babes, A., Neacsu, C., Sauer, S. K., Eberhardt, M., Schnölzer, M., Lasitschka, F., Lasischka, F., Neuhuber, W. L., Kichko, T. I., Konrade, I., Elvert, R., *et al.* (2012) Methylglyoxal modification of Nav1.8 facilitates nociceptive neuron firing and causes hyperalgesia in diabetic neuropathy. *Nat. Med.* **18,** 926–933 CrossRef Medline
33. Fleming, T., and Nawroth, P. P. (2014) Reactive metabolites as a cause of late diabetic complications. *Biochem. Soc. Trans.* **42,** 439–442 CrossRef Medline
34. Brenner, T., Fleming, T., Uhle, F., Silaff, S., Schmitt, F., Salgado, E., Ulrich, A., Zimmermann, S., Bruckner, T., Martin, E., Bierhaus, A., Nawroth, P. P., Weigand, M. A., and Hofer, S. (2014) Methylglyoxal as a new biomarker in patients with septic shock: an observational clinical study. *Crit. Care* **18,** 683 CrossRef Medline
35. Schmeisser, S., Priebe, S., Groth, M., Monajembashi, S., Hemmerich, P., Guthke, R., Platzer, M., and Ristow, M. (2013) Neuronal ROS signaling rather than AMPK/sirtuin-mediated energy sensing links dietary restriction to lifespan extension. *Mol. Metab.* **2,** 92–102 CrossRef Medline
36. Schulz, T. J., Zarse, K., Voigt, A., Urban, N., Birringer, M., and Ristow, M. (2007) Glucose restriction extends *Caenorhabditis elegans* life span by inducing mitochondrial respiration and increasing oxidative stress. *Cell Metab.* **6,** 280–293 CrossRef Medline
37. Zarse, K., Schmeisser, S., Groth, M., Priebe, S., Beuster, G., Kuhlow, D., Guthke, R., Platzer, M., Kahn, C. R., and Ristow, M. (2012) Impaired insulin/IGF1 signaling extends life span by promoting mitochondrial L-proline catabolism to induce a transient ROS signal. *Cell Metab.* **15,** 451–465 CrossRef Medline
38. Vázquez-Manrique, R. P., Farina, F., Cambon, K., Dolores Sequedo, M., Parker, A. J., Millán, J. M., Weiss, A., Déglon, N., and Neri, C. (2016) AMPK activation protects from neuronal dysfunction and vulnerability across nematode, cellular and mouse models of Huntington's disease. *Hum. Mol. Genet.* **25,** 1043–1058 CrossRef Medline
39. Mendler, M., Riedinger, C., Schlotterer, A., Volk, N., Fleming, T., Herzig, S., Nawroth, P. P., and Morcos, M. (2017) Reduction in ins-7 gene expression in non-neuronal cells of high glucose exposed *Caenorhabditis elegans* protects from reactive metabolites, preserves neuronal structure and head motility, and prolongs lifespan. *J. Diabetes Complications* **31**, 304–310 CrossRef Medline
40. Timmons, L., Court, D. L., and Fire, A. (2001) Ingestion of bacterially expressed dsRNAs can produce specific and potent genetic interference in *Caenorhabditis elegans*. *Gene* **263,** 103–112
41. Winder, W. W. (2008) Can patients with type 2 diabetes be treated with 5′-AMP-activated protein kinase activators? *Diabetologia* **51,** 1761–1764 CrossRef Medline
42. Mello, C. C., Kramer, J. M., Stinchcomb, D., and Ambros, V. (1991) Efficient gene transfer in *C. elegans*: extrachromosomal maintenance and integration of transforming sequences. *EMBO J.* **10,** 3959–3970 Medline
43. Schnabel, H., and Schnabel, R. (1990) An organ-specific differentiation gene, pha-1, from *Caenorhabditis elegans*. *Science* **250,** 686–688 CrossRef Medline
44. Granato, M., Schnabel, H., and Schnabel, R. (1994) pha-1, a selectable marker for gene transfer in *C. elegans*. *Nucleic Acids Res.* **22,** 1762–1763 CrossRef Medline
45. Altun-Gultekin, Z., Andachi, Y., Tsalik, E. L., Pilgrim, D., Kohara, Y., and Hobert, O. (2001) A regulatory cascade of three homeobox genes, ceh-10, ttx-3 and ceh-23, controls cell fate specification of a defined interneuron class in *C. elegans*. *Development* **128**, 1951–1969 Medline
46. Schumacher, B., Schertel, C., Wittenburg, N., Tuck, S., Mitani, S., Gartner, A., Conradt, B., and Shaham, S. (2005) *C. elegans* ced-13 can promote apoptosis and is induced in response to DNA damage. *Cell Death Differ.* **12**, 153–161 CrossRef Medline
47. Mendler, M., Schlotterer, A., Morcos, M., and Nawroth, P. P. (2012) Understanding diabetic polyneuropathy and longevity: what can we learn from the nematode *Caenorhabditis elegans*? *Exp. Clin. Endocrinol. Diabetes* **120,** 182–183 CrossRef Medline
48. Mendler, M., Schlotterer, A., Ibrahim, Y., Kukudov, G., Fleming, T., Bierhaus, A., Riedinger, C., Schwenger, V., Herzig, S., Hecker, M., Tyedmers, J., Nawroth, P. P., and Morcos, M. (2015) daf-16/FOXO and glod-4/glyoxalase-1 are required for the life-prolonging effect of human insulin under high glucose conditions in *Caenorhabditis elegans*. *Diabetologia* **58**, 393–401 CrossRef Medline
49. Abramoff, M. D., Magelhaes, P. J., and Ram, S. J. (2004) Image processing with ImageJ. *Biophotonics Int.* **11,** 36–42
50. Dhawan, A., Bajpayee, M., Pandey, A. K., and Parmar, D. (2003) *Protocol for the single cell gel electrophoresis/comet assay for rapid genotoxicity assessment*. Industrial Toxicology Research Centre, Lucknow, India
51. Park, S., Choi, S., and Ahn, B. (2016) DNA strand breaks in mitotic germ cells of *Caenorhabditis elegans* evaluated by comet assay. *Mol. Cells* **39,** 204–210 CrossRef Medline
52. Imanikia, S., Galea, F., Nagy, E., Phillips, D. H., Stürzenbaum, S. R., and Arlt, V. M. (2016) The application of the comet assay to assess the genotoxicity of environmental pollutants in the nematode *Caenorhabditis elegans*. *Environ. Toxicol. Pharmacol.* **45,** 356–361 CrossRef Medline

53. Dmitrieva, N. I., Cui, K., Kitchaev, D. A., Zhao, K., and Burg, M. B. (2011) DNA double-strand breaks induced by high NaCl occur predominantly in gene deserts. *Proc. Natl. Acad. Sci. U.S.A.* **108,** 20796–20801 CrossRef Medline
54. Hartmann, S., Okun, J. G., Schmidt, C., Langhans, C. D., Garbade, S. F., Burgard, P., Haas, D., Sass, J. O., Nyhan, W. L., and Hoffmann, G. F. (2006) Comprehensive detection of disorders of purine and pyrimidine metabolism by HPLC with electrospray ionization tandem mass spectrometry. *Clin. Chem.* **52,** 1127–1137
55. CycLex Co., Ltd. (2016) *Cyclex AMPK Kinase Assay Kit User Manual*, CycLex Co., Ltd., Nagano, Japan
56. Black, S. L., Black, M. J., and Mangum, J. H. (1978) A rapid assay for 5-amino-4-imidazelecar amide ribotide transformylase. *Anal. Biochem.* **90,** 397–401 CrossRef Medline
57. Tötemeyer, S., Booth, N. A., Nichols, W. W., Dunbar, B., and Booth, I. R. (1998) From famine to feast: the role of methylglyoxal production in *Escherichia coli*. *Mol. Microbiol.* **27,** 553–562 CrossRef Medline